Article

Cell Host & Microbe

Viral Spread to Enteric Neurons Links Genital HSV-1 Infection to Toxic Megacolon and Lethality

Graphical Abstract

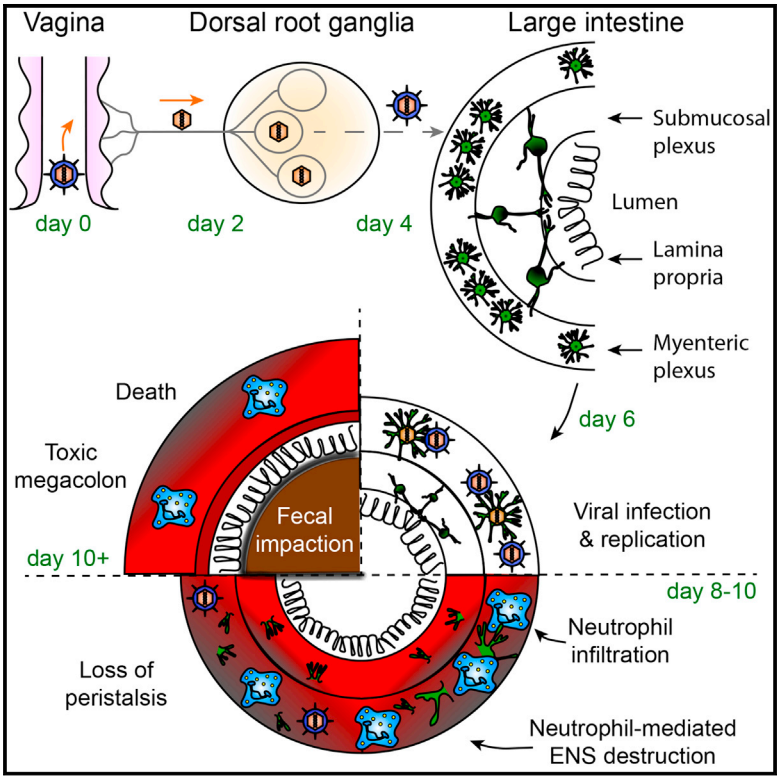

Highlights

- HSV-1-associated lethality in mice correlates with severe fecal and urinary retention
- HSV-1 spreads from nociceptors in the vagina to the enteric nervous system (ENS)
- Viral replication in the ENS leads to inflammation and neutrophil recruitment
- Neutrophil-mediated destruction of the ENS leads to lethality from genital herpes

Authors

William Khoury-Hanold, Brian Yordy, Philip Kong, ..., Alexandra Ralevski, Tamas L. Horvath, Akiko Iwasaki

Correspondence

akiko.iwasaki@yale.edu

In Brief

Genital herpesvirus infections cause urinary and gastrointestinal retention, which is poorly understood. Using a mouse model of genital infection, Khoury-Hanold et al. demonstrate that HSV spreads via nociceptors to the enteric nervous system (ENS). The resulting neutrophil-mediated ENS destruction and loss of peristalsis lead to toxic megacolon and death.

Accession Numbers

GSE74215

Khoury-Hanold et al., 2016, Cell Host & Microbe *19*, 788–799
June 8, 2016
http://dx.doi.org/10.1016/j.chom.2016.05.008

CellPress

Cell Host & Microbe
Article

Viral Spread to Enteric Neurons Links Genital HSV-1 Infection to Toxic Megacolon and Lethality

William Khoury-Hanold,[1] Brian Yordy,[1] Philip Kong,[1] Yong Kong,[2] William Ge,[1] Klara Szigeti-Buck,[3] Alexandra Ralevski,[3] Tamas L. Horvath,[3] and Akiko Iwasaki[1,4,*]
[1]Department of Immunobiology
[2]Department of Molecular Biophysics and Biochemistry, W.M. Keck Foundation Biotechnology Resource Laboratory
[3]Program in Integrative Cell Signaling and Neurobiology of Metabolism, Section of Comparative Medicine
[4]Howard Hughes Medical Institute
Yale University School of Medicine, New Haven, CT 06520, USA
*Correspondence: akiko.iwasaki@yale.edu
http://dx.doi.org/10.1016/j.chom.2016.05.008

SUMMARY

Herpes simplex virus 1 (HSV-1), a leading cause of genital herpes, infects oral or genital mucosal epithelial cells before infecting the peripheral sensory nervous system. The spread of HSV-1 beyond the sensory nervous system and the resulting broader spectrum of disease are not well understood. Using a mouse model of genital herpes, we found that HSV-1-infection-associated lethality correlated with severe fecal and urinary retention. No inflammation or infection of the brain was evident. Instead, HSV-1 spread via the dorsal root ganglia to the autonomic ganglia of the enteric nervous system (ENS) in the colon. ENS infection led to robust viral gene transcription, pathological inflammatory responses, and neutrophil-mediated destruction of enteric neurons, ultimately resulting in permanent loss of peristalsis and the development of toxic megacolon. Laxative treatment rescued mice from lethality following genital HSV-1 infection. These results reveal an unexpected pathogenesis of HSV associated with ENS infection.

INTRODUCTION

Herpesvirus infections are among the most common human viral infections in the world and persist for the life of the host (Virgin et al., 2009). Herpes simplex virus 1 and 2 (HSV-1 and HSV-2, respectively) infect the epithelial cells of the oral or genital mucosa before infecting the peripheral sensory nervous system. Within the dorsal root ganglia (DRG), they establish a latent infection that periodically reactivates to spread to the next susceptible individual. The successful implementation of this strategy requires that these viruses evade immune clearance and avoid causing excessive damage to host tissues. This is particularly important given that sensory neurons are non-renewable.

Historically, HSV-1 and HSV-2 are associated with oral and genital herpes, respectively. However, in many Western nations, HSV-1 recently surpassed HSV-2 as the leading cause of genital herpes infections (Malkin, 2004). Furthermore, the World Health Organization estimates that, in addition to the 417 million people with genital HSV-2 infections, there are ~140 million people living with genital HSV-1 infections (Looker et al., 2015a, 2015b). Following genital herpes infection, patients typically report recurrent, painful lesions that develop on and around the genitals, although viral reactivation and shedding also frequently occur in the absence of these symptoms (Wald et al., 1995). Despite the high prevalence of genital HSV-1 and HSV-2 infections, the ability of these viruses to spread beyond the sensory nervous system and the resulting broader spectrum of disease is not well understood.

Primary genital HSV-2 infections cause acute sensory defects, urinary retention, and constipation (Caplan et al., 1977; Goodell et al., 1983). Despite the fact that up to 15% of women report urinary retention following HSV-2 infection (Whitely et al., 1998), the exact mechanism remains unclear. Price and Notkins hypothesized that if a neurotropic virus spread to and replicated within the peripheral autonomic ganglia, this might result in further viral spread to the innervated "target" tissue and subsequent disruption in neuronal signaling or tissue atrophy due to lack of innervation (Price, 1977). Any of these scenarios would be predicted to negatively impact normal tissue function.

Although humans are the only natural hosts for HSV-1 and HSV-2, mouse models of genital HSV infection mimic some aspects of human disease, including urinary bladder retention (Parr and Parr, 2003; Reinert et al., 2012). In the current study, we used this model to investigate viral spread throughout the peripheral nervous system and its impact on the corresponding innervated tissues. We found that following infection of DRG sensory neurons, HSV-1 spreads to the enteric nervous system (ENS) and causes neutrophil-mediated neuronal damage leading to the loss of intestinal peristalsis and the development of toxic megacolon. Comparing the transcriptomes of the infected DRG and intestinal musculara, which contains the ENS, we showed that viral gene transcription is limited and incomplete in the DRG, whereas the viral genome is fully transcribed in the gut wall. Finally, mice treated with a laxative or a neutrophil-depleting antibody were protected from lethal HSV-1 infection. These results implicate enteric neuron infection and destruction in the disease pathogenesis of genital herpes, highlight the distinct consequences of a tissue-mismatched response to an

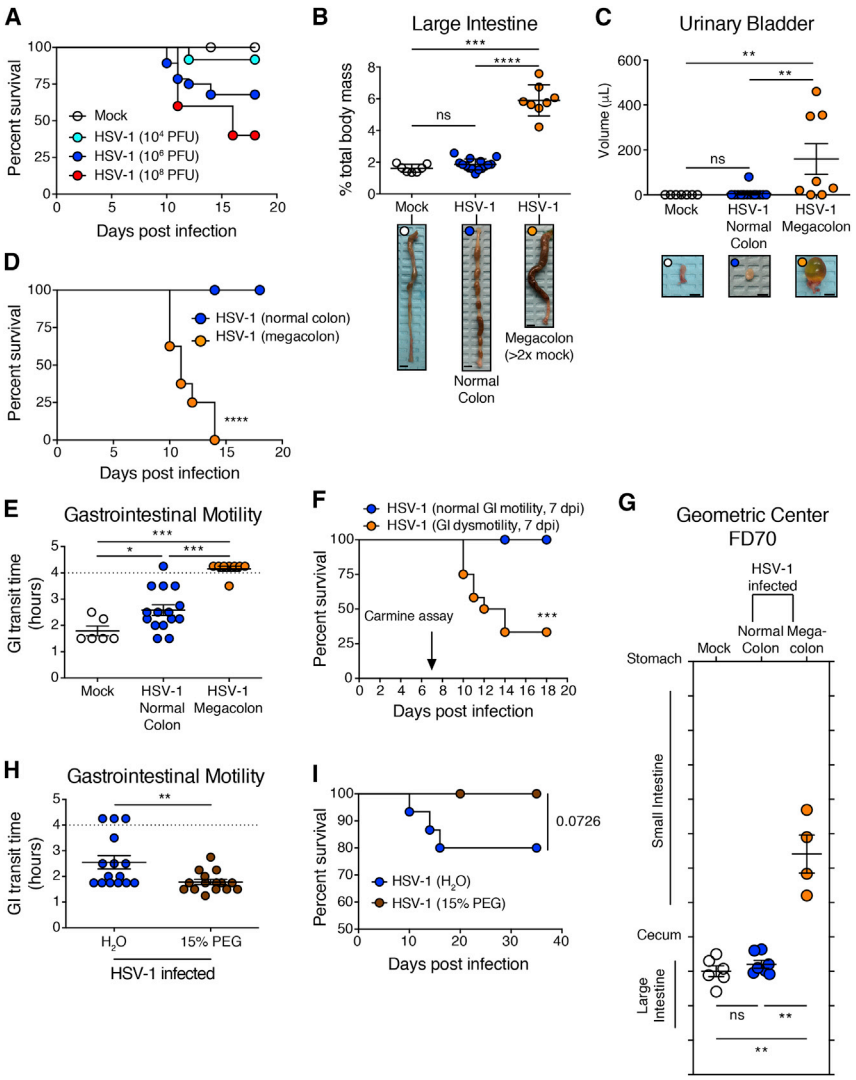

Figure 1. Genital HSV-1 Infection Leads to Toxic Megacolon

(A) Survival of mice infected with either 10^4, 10^6, or 10^8 PFU of HSV-1 intravaginally (i.vag).

(B and C) Mass of the large intestine normalized to total body mass (B) and volume of the urinary bladder (C) were recorded at the pre-moribund stage. Mice with megacolon (defined as a >2-fold increase in the mass of the large intestine compared to control mice) are segregated and depicted as orange dots for ease of comparison. Representative images depicting megacolon and urinary bladder retention are shown below each group. Scale bars represent 5 mm.

(D) Survival of mice infected with 10^6 PFU HSV-1 from (A), segregating mice with megacolon at time of death.

(E) Gastrointestinal (GI) transit time was determined 7 d.p.i. by measuring the length of time required to pass 300 μL of 6% (w/v) carmine red solution administered by oral gavage.

(F) Survival data from (A) segregating mice with GI dysmotility 7 d.p.i.

(G) The fluorescence geometric center of a fed bolus of FITC-Dextran (70 kDa) dye was calculated based on the percentage of the dye distribution along the entire GI tract.

(H and I) Starting on day 0, 15% (w/v) polyethylene glycol (PEG; MiraLAX) was administered via the drinking water to HSV-1-infected mice and GI transit time (H) and survival (I) were recorded as described above.

Data are shown as mean ± SEM and are pooled from two to six independent experiments totaling at least five mice per group. Statistical significance was measured by a log-rank (Mantel-Cox) test (D, F, and I) or by a Mann-Whitney test (exact) (B, C, E, G, and H); *$p < 0.05$, **$p < 0.01$, ***$p < 0.001$, ****$p < 0.0001$. The dotted line represents the limit of detection. See also Figure S1.

otherwise non-lethal virus, and suggest a possible expansion of the disease spectrum for HSV in humans.

RESULTS

Genital Herpes Infection Causes Colonic Dysmotility and Megacolon

HSV-1 is now the leading cause of genital herpes infections in many Western nations (Malkin, 2004), but its disease spectrum is poorly understood (Looker et al., 2015a). Therefore, we used a mouse model of genital HSV-1 infection to study disease pathogenesis. Following vaginal infection with 10^4 plaque-forming units (PFU), 10^6 PFU, or 10^8 PFU of HSV-1, ~10%, 30%, or 60% of infected mice succumbed to infection, respectively (Figure 1A). Viral loads in the vaginal mucosa of mice infected with either 10^6 or 10^8 PFU HSV-1 were identical 1 day postinfection (d.p.i.) and did not predict lethality (Figures S1A–S1C). We decided to use 10^6 PFU HSV-1, because this allowed us to study the susceptible and resistant mice with a single inoculum dose.

Prior reports show that mice develop hindlimb paralysis following genital HSV-2 infection (Fleck et al., 1993; Parr et al., 1994). Consistent with previous studies (Reinert et al., 2012), we detected both viral antigen (Figure S1D) and replication-competent virus in the brain stems (Figure S1F) of HSV-2-infected mice, indicating that CNS infection occurs after HSV-2 infection. In contrast, we did not observe hindlimb paralysis in HSV-1-infected C57BL/6 mice at any dose tested (data not shown). Further, we did not detect viral antigen, signs of inflammation, or replication-competent virus in the brain stem of HSV-1-infected mice (Figures S1D and S1E) (Yordy et al., 2012), suggesting an alternate pathogenesis. Instead, a surprising correlate of lethality was that mice infected with HSV-1 developed toxic megacolon, which we defined as a > 2-fold increase in the weight of the colon due to fecal retention (Figure 1B), as well as urinary bladder retention (Figure 1C). To delineate the two groups, HSV-1-infected mice that develop megacolon will be depicted by orange symbols, whereas infected mice that do not develop megacolon and survive the infection will be depicted as blue symbols, where applicable. Notably, all the mice that died of HSV-1

infection developed megacolon (Figure 1D). Mice infected with HSV-2 also uniformly developed megacolon and urinary bladder retention following vaginal infection (Figures S1G and S1H).

To formally assess gastrointestinal (GI) motility, we measured the time required for a dye (carmine red), administered by oral gavage, to transit the length of the GI tract. By 7 d.p.i., we observed a significant increase in GI transit time (Figure 1E), indicating a defect in peristalsis. This GI dysmotility predicted subsequent mortality in a majority of mice (Figure 1F). To determine where along the GI tract this defect in peristalsis occurs, mice were fed a non-absorbable and non-digestible high-molecular-weight fluorescein isothiocyanate (FITC)-dextran (FD70) (Tsukamoto et al., 2011). In control mice, peak fluorescence activity was detected in the proximal and mid sections of the large intestine 2.5 hr after oral feeding of FD70 (Figure 1G). In contrast, HSV-1-infected mice displayed an accumulation of FD70 in the small intestine, suggesting a defect in the passage of luminal contents from the small intestine to the large intestine (Figure 1G). Taken together, these data demonstrate that genital HSV infection results in severe colonic dysmotility and megacolon.

Lethality Following Genital HSV-1 Infection Is Due to Toxic Megacolon

Our data indicated that GI dysmotility and the development of megacolon are correlated with mortality (Figure 1D). To test the causality of megacolon in lethality, we treated mice with an osmotic laxative by replacing the drinking water with a 15% (w/v) polyethylene glycol (PEG; MiraLAX) solution. Laxative treatment fully restored normal GI transit times in HSV-1-infected mice (Figure 1H) and resulted in a 100% survival rate (Figure 1I). On the other hand, laxative treatment did not rescue mice from lethal HSV-2 infection, despite restoration of normal GI transit times (Figures S1I and S1J). Taken together, these data indicate that the primary cause of death following genital HSV-1 infection is due to not encephalitis but rather toxic megacolon.

HSV-1 Infection Spreads to the Enteric Nervous System

Following vaginal infection, HSV-2 spreads to distal neuronal sites such as the sensory neurons of the DRG and the autonomic neurons of the paracervical ganglia and the sympathetic chain (Parr and Parr, 2003). However, the pattern of HSV-1 spread is unknown. It was also unclear whether HSV-1-induced megacolon was the result of viral spread to the spine and subsequent disruption in signaling to the intestines or whether the virus could spread directly to the intestines and disrupt autonomic signaling in situ. To address this question, we measured viral titers from multiple tissues following vaginal HSV-1 infection (Figure 2A). Within 2 days, HSV-1 spread from the vagina to the urinary bladder, paracervical ganglia, and DRG. Subsequently, HSV-1 spread to the lumbosacral and, to a lesser extent, the cervical-thoracic spinal cord. Notably, the highest viral load was detected late during infection in the large intestine. Virus was not routinely detected in the terminal ileum of the small intestine, the liver, or the sympathetic chain. These data indicated that viral dissemination, while broad, was not systemic and was limited to a set of tissues linked by adjacent epithelial cells or neuron-to-neuron connections.

Given the high viral titers detected in the large intestine, we next examined which cell types were infected with HSV-1. Immunohistochemistry revealed that HSV antigen was confined to the ENS, specifically the myenteric ganglia of the longitudinal muscle, and was not present in either the submucosal or the epithelial layers (Figure S2A). Abundant mononuclear and polymorphonuclear leukocyte recruitment to the longitudinal muscle was also evident in the infected large intestine (Figure S2A). To visualize the infected myenteric plexus more clearly, we imaged the large intestine longitudinal muscle, which contains the myenteric plexuses, by whole-mount microscopy. Mock- and HSV-1-infected mice with normal colons had a similar distribution of myenteric neurons and glial cells with no detectable HSV-1 antigen (Figures 2B and S2B). However, mice with viral-induced megacolon showed a clear presence of HSV-1 within the enteric ganglia at 7 d.p.i. (Figure 2B). By 9 d.p.i., HSV-1 staining was mostly absent (Figure 2B), which coincided with the eventual elimination of the virus from the large intestine at later time points (Figure 2A). Strikingly, we also observed a paucity of neurons throughout the mid and distal colon (Figure 2B). Indeed, electron microscopy of the myenteric plexus 6 d.p.i. revealed swollen mitochondria (arrows) and mature viral particles (arrowheads) within degenerating neurons (Figures 2C1–2C4) (Chu-Wang and Oppenheim, 1978). Furthermore, mature viral particles were occasionally observed in adjacent smooth muscle cells (Figure 2C5). Finally, we observed phagocytic polymorphonuclear cells engulfing infected cell debris (Figure 2C6). Taken together, these results indicate that HSV-1 infects the autonomic ganglia of the ENS and the surrounding smooth muscle, resulting in neuronal damage. These data suggest that GI dysmotility is due to either immune-mediated inhibition of peristalsis (Boeckxstaens and de Jonge, 2009) or viral-induced neuronal cell death.

Nociceptors Are Necessary for HSV-1 Spread to the ENS

Given that HSV-1 was detected in multiple neuronal and non-neuronal sites, we next sought to determine the route by which virus spreads from the vagina to the ENS. To examine whether nociceptors are required for HSV-1 spread to the large intestine, we used resiniferatoxin (RTX), a capsaicin analog that selectively binds the transient receptor potential cation channel subfamily V member 1 (TRPV1) receptor, to ablate peripheral nociceptors (Riol-Blanco et al., 2014). Treatment with RTX abrogated noxious heat sensation (Figure S3A), thus indicating successful nociceptor ablation. While RTX treatment did not affect HSV-1 infection and replication within the vaginal epithelium (Figure 3A), it prevented virus from reaching the DRG (Figure 3B). Subsequent viral spread to the large intestine (Figure 3C) and viral-induced GI dysmotility, megacolon, and mortality (Figures 3D–3F) were also prevented following RTX treatment. These data indicated that neuronal spread (rather than epithelial cell spread) via peripheral TRPV1$^+$ nociceptors is required for HSV-1 to spread from the vagina to the large intestine. Furthermore, blocking HSV-1 entry into the peripheral sensory nervous system prevented viral-induced GI dysmotility and megacolon.

Robust Viral Gene Transcription in the Intestinal Musculara, but Not the DRG

Our findings suggested that enteric neurons are susceptible to damage and elimination during an HSV-1 infection (Figure 2). In contrast, sensory DRG neurons are resistant to viral-induced

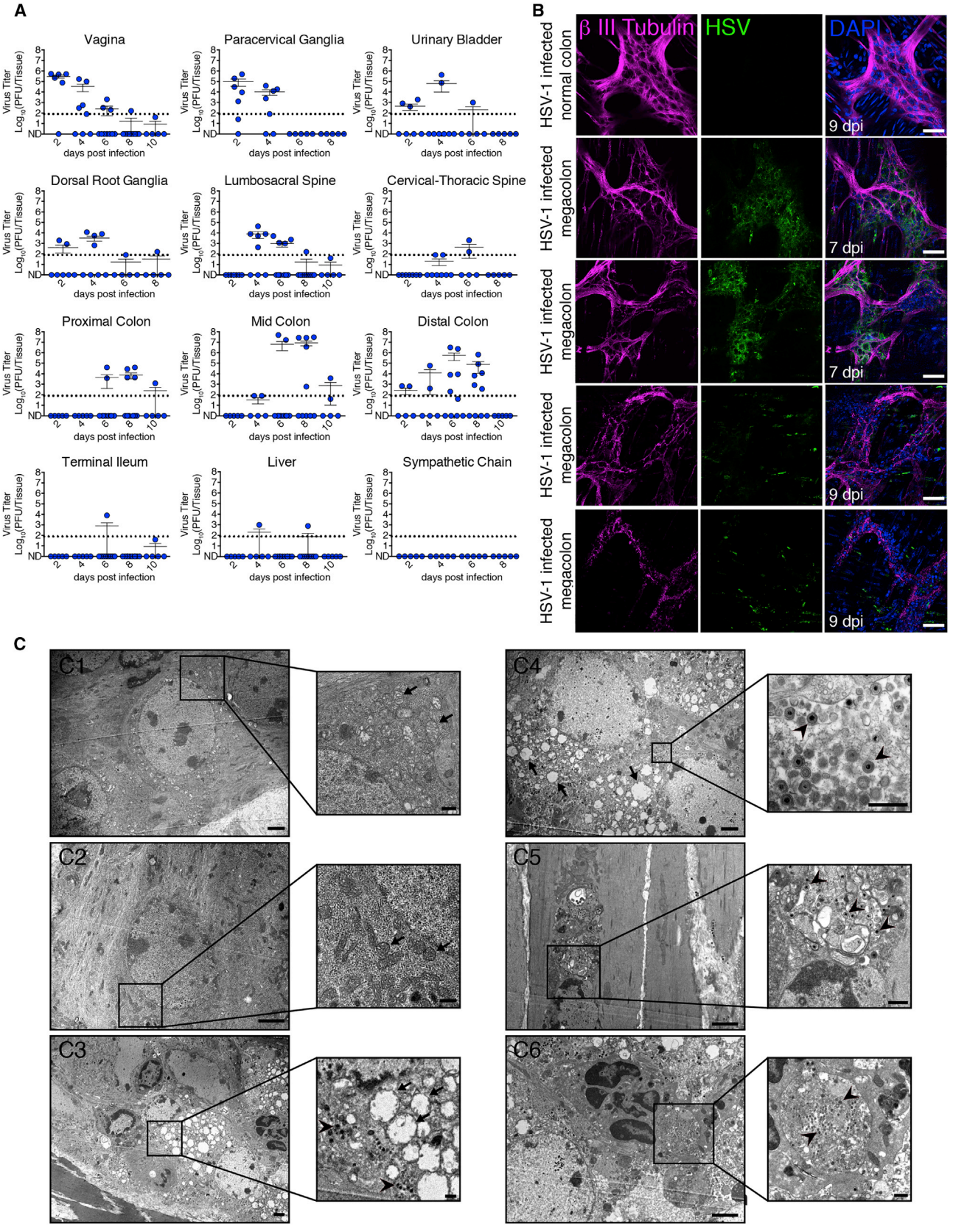

(legend on next page)

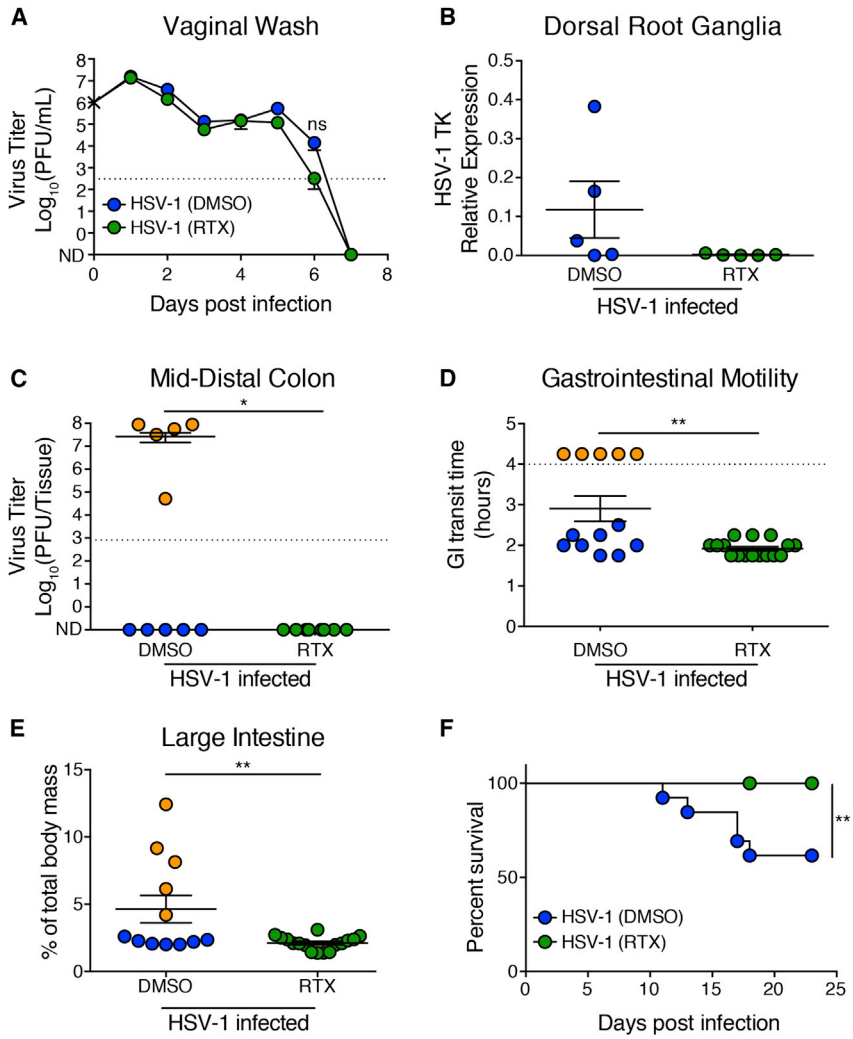

Figure 3. HSV-1 Spreads to the ENS via Nociceptors

Mice were treated with vehicle (DMSO) or resiniferatoxin (RTX) to ablate peripheral TRPV1$^+$ nociceptive-neurons.

(A) Viral titers in the vaginal wash were measured by plaque assay.

(B) Four d.p.i., HSV-1 genome abundance in the DRG was determined by qPCR and normalized to the mouse *Tert* gene.

(C) Viral titers in the large intestine at 7 d.p.i.

(D) GI motility was determined at 1.5 weeks post infection as described in Figure 1.

(E and F) mass of the large intestine at necropsy (E) and survival (F) were recorded. Mice with megacolon are highlighted orange.

Data are shown as mean ± SEM and are pooled from one to two independent experiments totaling 5–16 mice per group. Statistical significance was measured by a Mann-Whitney test (exact) (A–E) or by a log-rank (Mantel-Cox) test (F); *p < 0.05, **p < 0.01. The dotted line represents the limit of detection. See also Figure S3.

cell death and are not eliminated by HSV infection (Yordy et al., 2012) or cytotoxic T cell infiltration (Simmons and Tscharke, 1992). This raised the intriguing possibility that there are tissue-specific strategies that mitigate neuronal damage in the DRG but are absent in the ENS. To better understand these underlying differences, we performed RNA sequencing (RNA-seq) analysis on the DRG and the large intestine musculara containing the ENS 6 days after HSV-1 infection. To analyze the viral transcriptome, sequenced reads from each tissue were first mapped to the human herpesvirus 1 genome (GenBank: NC_001806.1). The number of reads mapping to each nucleotide position are displayed as a Circos plot (Krzywinski et al., 2009) (Figure 4A). Robust and complete viral transcription through all known HSV-1 coding regions was observed in the large intestine musculara of mice with virus-induced megacolon (Figure 4A, outer track). However, sequence analysis of the infected DRGs revealed that viral transcription through multiple coding regions was less robust or, in some cases, undetectable (Figure 4A, inner track). Furthermore, when compared to mock levels, approximately half of the beta (early) and gamma (late) genes failed to reach statistical significance in the DRG (Figure 4B), whereas all HSV-1 genes were significantly expressed in the large intestine musculara (Figure 4C). These data indicate that HSV-1 transcription and replication is restricted in sensory, but not enteric, neurons.

Distinct Inflammatory Consequences of HSV-1 Infection in the DRG versus the Large Intestine Musculara

We next sought to analyze the host response to HSV-1 infection. Comparing control mice to those with virus-induced megacolon, we observed 2,884 downregulated and 2,882 upregulated genes that reached statistical significance in the large intestine

Figure 2. HSV-1 Infection of the Enteric Ganglia Results in Neuronal Damage

(A) At indicated days postinfection, mice were sacrificed and viral titers were measured from whole-tissue homogenates. The dotted line represents the limit of detection. Data are shown as mean ± SEM and are pooled from three independent experiments totaling five to ten mice per time point.

(B) Whole-mount microscopy images of the large intestine musculara at indicated days postinfection (dpi). Scale bars represent 50 μm.

(C) Electron microscopy images of the large intestine myenteric plexus 6 d.p.i. (1 and 2) Mock-infected mice with normal mitochondrial ultrastructure (arrows). (3 and 4) HSV-1-infected neurons exhibit features that are characteristic of degenerating and dying neurons (Chu-Wang and Oppenheim, 1978), such as cytoplasmic vacuolization and dilated mitochondria (arrows). (3–6) Viral particles (arrowheads) are also evident within neurons (3 and 4), smooth muscle cells (5), and within the phagosome of a polymorphonuclear cell (6). Polymorphonuclear cells adjacent to infected neurons (3 and 6). Scale bars represent 2 μm and 100 nm in panels and inset, respectively. Immunofluorescence and EM images are representative of at least two independent experiments.

See also Figure S2.

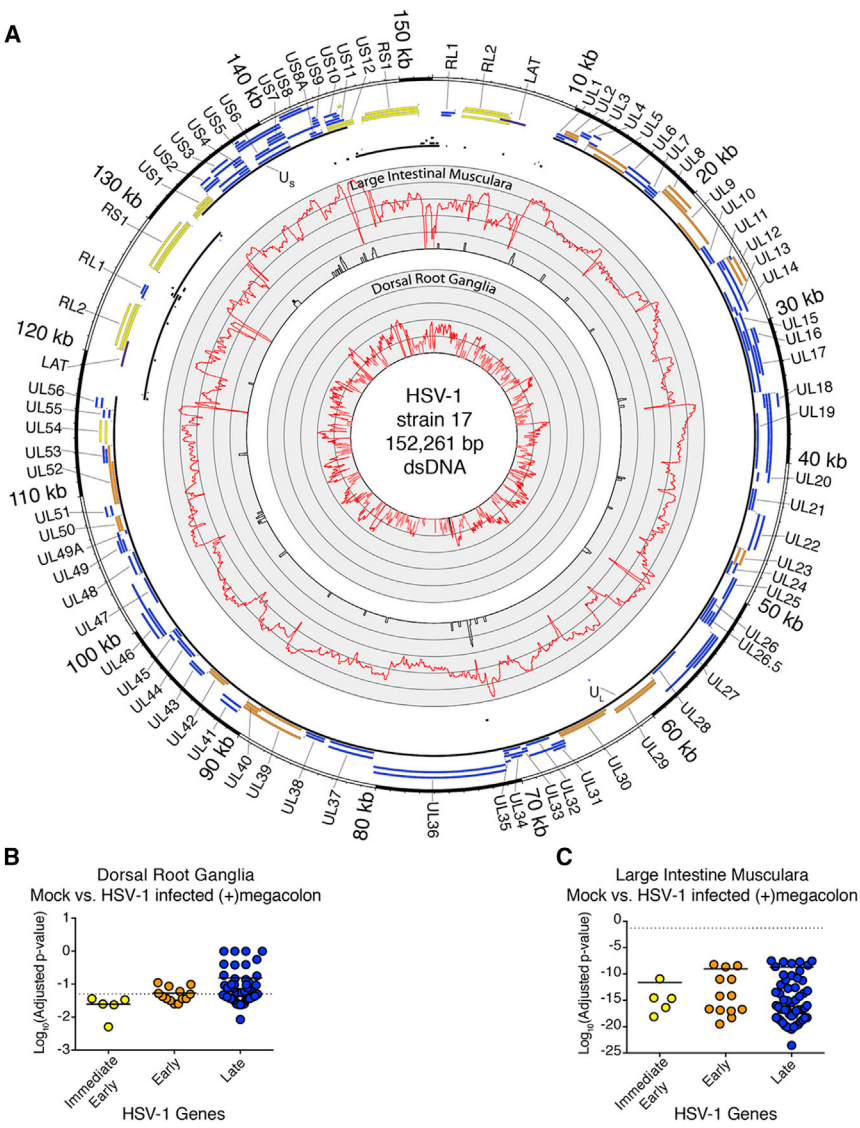

Figure 4. HSV-1 Gene Transcription in the Large Intestine Musculara and the DRG

The large intestine musculara and DRG were isolated 6 d.p.i. and subjected to RNA sequencing analysis as described in Experimental Procedures. (A) Circos plot displaying the frequency of mapped sequence reads to each nucleotide position of the HSV-1 genome on a $\log_2$ scale. Representative samples of mock-infected (black lines) or HSV-1-infected (red lines) tissues (inner track shows DRG; outer track shows large intestine musculara). The magnitude of mapped HSV-1 reads is depicted as light red lines, $<2^3$; dark red lines, $>2^3$. Yellow boxes represent alpha genes, orange boxes represent beta genes, blue boxes represent gamma genes, purple boxes represent the latency-associated transcripts (LATs), and black boxes represent non-coding regions such as repeat regions and origins of replication.

(B and C) Statistical significance of HSV gene expression compared to mock-infected tissues. The dotted line represents the cutoff for statistical significance (adjusted p value < 0.05).

musculara. Using Ingenuity Pathway Analysis (IPA) to categorize the downregulated genes, we observed that canonical pathways pertaining to neuronal signaling such as "calcium signaling," "axonal guidance signaling," and "cardiac β-adrenergic signaling" were enriched, which is consistent with a defect in autonomic neuronal signaling and smooth muscle peristalsis (Figure S4A). Indeed, genes encoding multiple neurotransmitter receptor subunits were significantly downregulated in the large intestine musculara following HSV-1 infection (Figure 5A). The most highly enriched upregulated pathways revealed a signature indicative of innate immune responses to viral infection such as pattern recognition receptor (PRR) and antigen receptor signaling (Figure S4A). Indeed, many interferon-stimulated genes (ISGs) and pro-inflammatory cytokines and chemokines were highly upregulated, including the neutrophil chemokines *Cxcl1*, *Cxcl2*, *Cxcl3*, and *Cxcl5* and their receptor, *Cxcr2* (Figure 5A).

By comparison, the transcriptional response in the HSV-1-infected DRG was muted: only 8 genes were significantly downregulated, and 473 genes were significantly upregulated. IPA canonical pathway analysis revealed a T cell signature within the infected DRGs (Figures S4B and 5B). In contrast to the intestinal musculara, only a limited number of chemokine genes were upregulated in the DRG, specifically those related to effector T cell (e.g., *Cxcl9*, *Cxcl10*) and monocyte (e.g., *Ccl2*) recruitment (Figure 5B). Notably, there was a paucity of genes encoding chemokines involved in neutrophil recruitment, ISGs, and innate sensors in the DRG. Taken together, these results suggest that in response to the same viral infection, these two tissues engage markedly different immune responses. Whereas signatures of T cell recruitment and activation dominate the DRG response, the intestinal musculara exhibits a hyper-inflammatory response conducive to leukocyte recruitment.

Neutrophils Contribute to Immunopathology and Megacolon

Our RNA-seq findings indicated that HSV-1 infection of the DRG and intestinal musculara resulted in two distinct host gene signatures. Therefore, we further analyzed the host response by assessing immune cell recruitment to these infected tissues by flow cytometry. In line with the robust T cell gene expression signature in both tissues following HSV-1 infection, we detected a modest increase in activated $CD4^+CD44^+$ and $CD8^+CD44^+$ T cells 6 d.p.i. (Figures S5A and S5B) and a significant increase by 9 d.p.i. in both the DRG and the large intestine musculara (Figures 6A and 6B). In addition, there was a significant increase in $CD25^+Foxp3^+$ regulatory T (Treg) cells in the large intestine musculara (Figure 6C) consistent with an excessive inflammatory environment. However, distinct patterns of leukocyte recruitment between the DRG and large intestine musculara emerged.

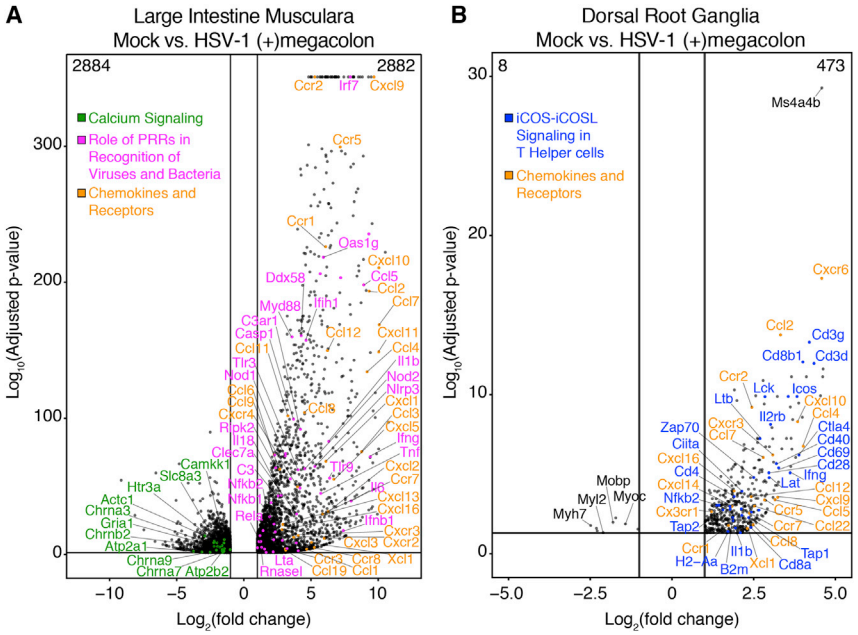

Figure 5. Host Transcriptional Response to HSV-1 Infection of the Large Intestine Musculara and DRG

(A and B) Volcano plots displaying the fold change and p value of differentially expressed genes (≥2-fold change and adjusted p value < 0.05) in the large intestine musculara (A) and DRG (B) in HSV-1-infected mice compared to mock-infected controls. Color-coded genes correspond to text and Figure S4.

By 9 d.p.i., with the exception of a modest increase in inflammatory monocytes and conventional dendritic cells (cDCs), the number of innate leukocytes in the DRG returned to baseline (Figures S5D–S5F and 6D–6F). In contrast, we observed a significant increase in the number of inflammatory monocytes, cDCs, natural killer (NK) cells, and neutrophils in the intestinal musculara (Figures S5D–S5G and 6D–6G).

Given the influx of inflammatory leukocytes into the infected large intestine (Figures S2A, S5, and 6), we hypothesized that HSV-1 infection of the ENS might result in disrupted enteric neuron signaling to smooth muscles via two non-mutually exclusive mechanisms: (1) viral replication (Kramer and Enquist, 2012) or inflammation (Boeckxstaens and de Jonge, 2009) would disrupt neuronal signaling, or (2) viral infection and replication would result in neuronal cell death. Both of these scenarios would ultimately result in GI dysmotility. Therefore, to begin to assess the potential role for immune-mediated GI dysmotility, we infected *Rag2*$^{-/-}$ mice with HSV-1 and determined that the adaptive immune system was dispensable for HSV-1-induded megacolon (Figure S5H) and lethality (Figure S5I). However, T and B cells were required for protection against a neuro-attenuated strain of HSV-1 (Figure S5I), as previously described (Leib et al., 2009). These data indicated that while the adaptive immune system is required for neuroprotection against HSV, it is not required for the immunopathology observed in the ENS following infection.

Given that neutrophils were recruited to the large intestine musculara, but not to the DRG (Figures 6G and S5G), we next sought to address their contribution to disease. Neutrophils were depleted using the anti-Ly6G (1A8) antibody (Daley et al., 2008) beginning 5 d.p.i. Neutrophil depletion had no effect on viral replication in the genital tract (Figure S6A). Furthermore, this treatment did not prevent viral infection of the large intestine (Figure S6B) and the development of HSV-1-induced GI dysmotility at 8 d.p.i. (Figure 7A). However, mice depleted of neutrophils were partially rescued from lethal HSV-1-induced mortality compared to immunoglobulin G (IgG)-treated controls (Figure 7B). In control IgG-treated mice, GI dysmotility at 8 d.p.i. predicted subsequent lethality in ~90% of mice (Figure 7B), whereas neutrophil-depletion improved the odds of surviving this episode of GI dysmotility by ~5-fold (Figure 7B). Surviving mice that suffered transient colonic dysmotility recovered normal GI motility 2 weeks after infection in the absence of neutrophils (Figure 7C). To explore how neutrophil-depleted mice recover GI motility following HSV-1 infection of the myenteric plexus, we used whole-mount microscopy to image the ENS. In the absence of neutrophils, the ENS remained intact, whereas the ganglia of control-treated mice were eliminated during infection (Figure 7D). These data indicate that in the absence of neutrophils, viral replication or inflammation in the musculara leads to a transient period of GI dysmotility, which eventually recovers following viral clearance. However, in the presence of neutrophils, further destruction of the ENS by neutrophils leads to toxic megacolon and death.

DISCUSSION

In this study, we demonstrate that HSV-1 infection in mice results in lethality due to toxic megacolon. Following replication in the vaginal epithelium, HSV-1 infects the innervating sensory neurons of the DRG. At this site, viral gene transcription was confined, leading to the induction of a small set of host-response genes that recruited and maintained T cells. In approximately one-third of infected mice, HSV-1 infection spread from the DRG to the ENS. Here, HSV-1 infection resulted in extensive viral gene transcription and viral replication. This led to the induction of a large number of host-response genes, including inflammatory chemokines. Consequently, neutrophils were recruited to the large intestine musculara and mediated the destruction of the enteric ganglia. In the absence of neutrophils, viral infection or inflammation led to a transient inhibition of peristalsis, which later recovered following viral clearance, and ultimately led to improved survival rates. Alternatively, chronic treatment with an osmotic laxative bypassed the need for an intact ENS and prevented the development of toxic megacolon and lethality. Our results indicate that distinct peripheral neuronal tissues vary in their capacity to restrict HSV-1 and limit

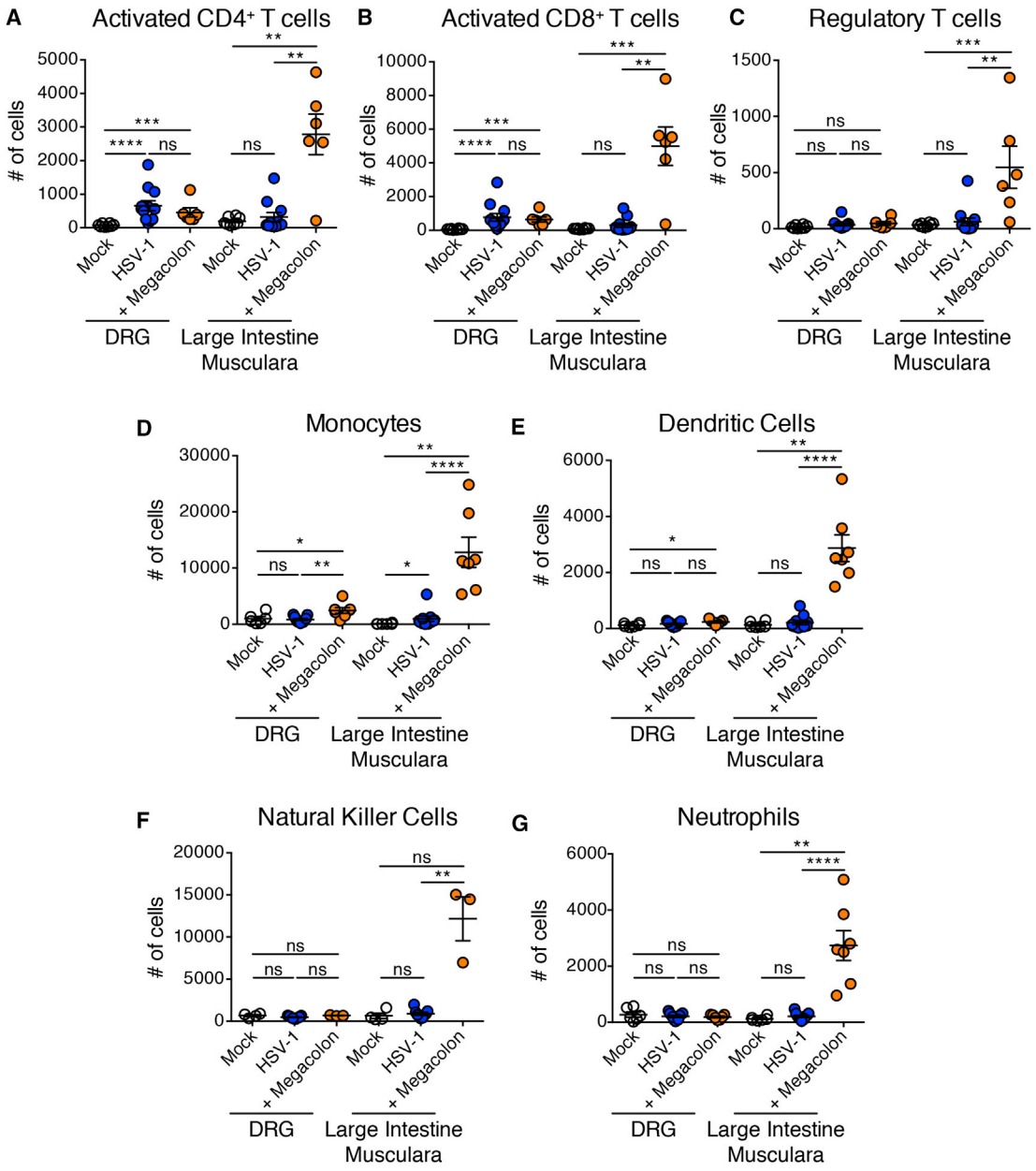

Figure 6. Distinct Cellular Recruitment to the DRG versus Large Intestine Musculara in Response to HSV-1

(A–G) The DRG and large intestine musculara were harvested and analyzed by flow cytometry 9 d.p.i. All samples were gated on live, CD45.2$^+$ cells. The number of (A) CD3$^+$CD4$^+$CD44$^+$ activated T helper cells, (B) CD3$^+$CD8$^+$CD44$^+$ activated cytotoxic T cells, (C) CD25$^+$Foxp3$^+$ regulatory T cells, (D) CD11b$^+$Ly6C$^+$ monocytes, (E) CD11c$^+$MHCII$^+$ dendritic cells, (F) NK1.1$^+$ natural killer cells, and (G) CD11b$^+$Ly6G$^+$ neutrophils are displayed. Data are shown as mean ± SEM and are pooled from two to three independent experiments totaling 4–18 mice per group. Statistical significance was measured by a Mann-Whitney test (exact), *p < 0.05, **p < 0.01, ***p < 0.001, ****p < 0.0001; ns, not significant.

See also Figure S5.

immunopathology, thus revealing an unexpected disease mechanism following genital herpes infection.

In contrast to our findings, previous studies have shown that BALB/c mice infected with HSV-1 develop lethal encephalitis following infection via the oral (Kastrukoff et al., 1986) or intraperitoneal routes (Lopez, 1975). However, this does not occur in C57BL/6 mice, which are generally more resistant to CNS disease (Kastrukoff et al., 1986; Lopez, 1975). Curiously, HSV-1 infected the vagus nerve following oral infection in BALB/c mice (Gesser and Koo, 1996; Gesser et al., 1994), leading to encephalitis. In these susceptible mice, the infected vagus nerve would provide the virus a direct neuronal path to both the brain stem and the ENS of the upper GI tract. However, following vaginal infection in C57BL/6 mice, HSV-1 must first infect sensory neurons before transmitting to sacral spinal neurons of the dorsal horns. We speculate that in a more resistant mouse strain,

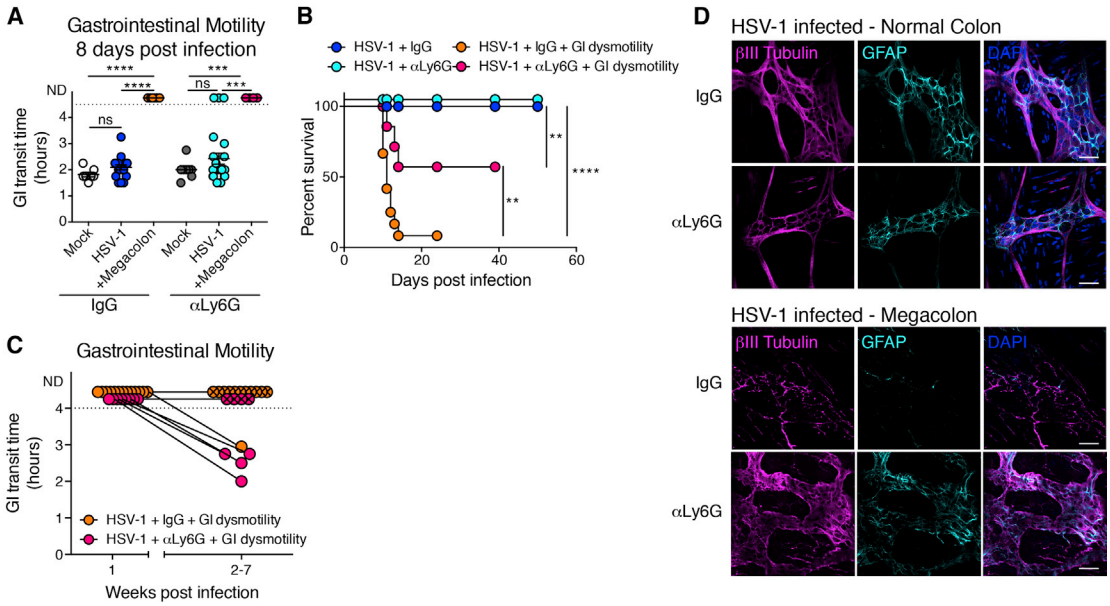

Figure 7. Depletion of Neutrophils Rescues Mice from HSV-1-Induced Mortality

Beginning 5 d.p.i., mice were treated with 500 μg anti-Ly6G neutrophil depleting antibody (1A8) or isotype control (IgG) every other day.

(A) 8 d.p.i., GI motility was determined as described in Figure 1.

(B) Survival of mice treated with anti-Ly6G neutrophil depleting antibody or IgG control. Mice are segregated into separate groups based on their GI motility status as shown in (A).

(C) At 2–7 weeks after infection, GI motility was re-assessed in those mice that had severe dysmotility at 8 d.p.i. "X" circles indicate that the mouse died before re-assessment could take place. Data are shown as mean ± SEM and are pooled from 4-5 independent experiments totaling 8–32 mice per group. Statistical significance was measured by a Mann-Whitney test (exact) (A) or by a log-rank (Mantel-Cox) test (B), *$p < 0.05$, **$p < 0.01$, ***$p < 0.001$, ****$p < 0.0001$; ns, not significant.

(D) Whole-mount microscopy images of the large intestine musculara showing enteric neurons (magenta), glial cells (teal), and nuclear DAPI staining (blue) at 9 d.p.i. Scale bars represent 50 μm. Data are representative of at least two mice per group.

See also Figure S6.

such as C57BL/6, HSV-1 is restricted from spreading from the lumbosacral spinal cord to the brain stem due to cell-intrinsic (Yordy et al., 2012) or cell-extrinsic (Johnson et al., 2008; Knickelbein et al., 2008) mechanisms and instead spreads to the ENS.

Our data indicate that TRPV1$^+$ nociceptors are required for viral spread from the genital tract to the ENS of the large intestine. These results support two possible routes that might result in the transfer of virus from the genital tract to the ENS. A first possibility is that HSV-1 is transported via the DRG to the lumbosacral spinal cord. From there, virus could spread transsynaptically to any one of several spinal neurons that provide extrinsic signaling to the intestines (Brookes et al., 2013). The second possible route predicts that HSV-1 infects a subpopulation of nociceptive DRG neurons that simultaneously extend axons into both genitourinary and intestinal tissues (Chaban et al., 2007; Christianson et al., 2007). Therefore, these "dichotomizing" neurons provide a direct link for virus to transmit between the female reproductive tract and the large intestine. Future studies that clarify how the virus spreads from the DRG to the ENS might help to explain why only a subset of HSV-1-infected mice developed megacolon.

Comparing the HSV-1-infected DRG to the ENS, our transcriptome analysis revealed striking differences in both viral and host gene expression. Viral gene expression in the ENS was robust across all known coding regions of the genome. In the DRG, on the other hand, transcription through many coding regions was undetectable, and mRNA expression of many of the early and late genes failed reach statistical significance. This pattern of viral gene expression is indicative of abortive replication but may ultimately serve to limit the induction of pathological pro-inflammatory cytokines and chemokines, as seen in the large intestine musculara. Indeed, the DRG recruited activated T cells in response to infection, which are required to limit viral replication and cell death (Simmons and Tscharke, 1992) and restricted the entry of neutrophils (Figure 6G) (Stock et al., 2014). The intestinal musculara, on the other hand, supported the recruitment of both T cells and neutrophils. In this regard, it appears that the mechanisms controlling leukocyte recruitment to the gut wall are more similar to those of the skin or vagina (Shin and Iwasaki, 2013; Stock et al., 2014). Our data demonstrate the importance of barring neutrophil recruitment to the peripheral nervous system, given that lytic viral infection of the ENS is not the primary cause of neuronal destruction, and suggest it is the immunopathology inflicted by activated neutrophils that causes agangliosis and toxic megacolon. Surprisingly, neutrophil-depleted mice recovered from transient virus-induced or inflammation-induced GI dysmotility and ultimately restored motility in the large intestine. Understanding the process of neuronal repair and restoration in this model might shed light on the treatment of idiopathic gastrointestinal motility disorders.

Orally acquired HSV-1 can spread to multiple sensory and autonomic ganglia, thus demonstrating a broad neuronal tropism throughout the head, neck, and torso (Arbusow et al., 2010; Richter et al., 2009; Warren et al., 1978). Furthermore, studies have shown that both primary infection and reactivation of latent HSV-1 can cause paralysis of the vagus nerve (e.g., trouble swallowing and vocalizing) (Bachor et al., 1996) and herpes esophagitis (Canalejo Castrillero et al., 2010). However, the clinical prevalence and implications of HSV-1 infection in the sacral ganglia and ENS remain understudied. While small-scale studies have linked the presence of herpesvirus family members to chronic idiopathic pseudo-obstruction (CIPO), HSV is only occasionally detected in patient samples (De Giorgio et al., 2010; Debinski et al., 1997). A direct causal link between HSV infection and chronic intestinal motility disorders might be difficult to draw because the virus may be cleared from the ENS before the diagnosis is made. Our findings suggest that future clinical studies should assay patients for the presence of HSV at the onset of GI dysmotility before viral clearance takes place. Taken together, our current results and previous clinical evidence suggest an underappreciated role for HSV infection of the ENS in intestinal motility disorders in humans, and extends the disease spectrum of HSV beyond the genital mucosa and sensory nervous system.

EXPERIMENTAL PROCEDURES

Mice

C57BL/6 (B6) female mice were purchased from Charles River Laboratories or the National Cancer Institute and subsequently bred and housed at Yale University. *Rag2*$^{-/-}$ mice were bred and housed at Yale University. All animal procedures were performed in compliance with Yale Institutional Animal Care and Use Committee protocols.

Viruses and In Vivo Infections

Wild-type (Δ68HR) HSV-1 (strain 17syn+) and beclin binding domain deletion virus (Δ68H) (strain 17syn+) were kind gifts from Dr. David Leib (Geisel School of Medicine at Dartmouth) (Leib et al., 2009). Wild-type HSV-2 (strain 186syn+) was a kind gift from Dr. David Knipe (Harvard Medical School). All HSV strains were maintained and propagated using Vero cells. In vivo infections were performed as previously described (Shin and Iwasaki, 2012). Briefly, 5- to 8-week-old female mice were treated with Depo-Provera (GE Healthcare). Five to seven days later, the vaginal lumen was cleared of mucous with a Calginate swab (Fischer Scientific) and 10 μL containing 10^6 PFU, unless otherwise noted, of virus were delivered into the vaginal lumen with a pipette. Viral titers from indicated homogenized tissues were determined by a standard plaque assay using Vero cells as described in Supplemental Experimental Procedures.

Measuring GI motility

To measure the total GI transit time, mice were orally gavaged with a 6% w/v carmine red (Sigma), 0.5% methocellulose, and 0.9% NaCl solution. Mice were monitored for at least 4.5 hr and the time required to pass the carmine red dye in the feces was recorded. Alternatively, GI motility was measured using a non-digestible, non-absorbable high-molecular-weight FITC-labeled dextran (FD70) as previously described (Tsukamoto et al., 2011). Briefly, mice were fed a 10-μL bolus of FD70 and sacrificed 2.5 hr later. The entire GI tract was dissected and separated into 13 sections: stomach, 8 sections of small intestine, cecum, and 3 sections of large intestine. The small and large intestines were each measured and divided into equal sections relative to their total lengths. The contents of each section were opened in a 1.5-mL Eppendorf tube with 800 μL PBS. After vigorous vortexing, the samples were clarified by centrifugation and fluorescence was measured from the supernatants on a SpectraMax M5 (Molecular Devices) fluorescence plate reader.

Treatment with Osmotic Laxative

At time of infection, the drinking water was replaced with a 15% w/v solution of MiraLAX (polyethylene glycol 3350, Bayer) for the duration of the experiment.

Isolation of Large Intestine Musculara and Whole-Mount Microscopy

The musculara of the large intestine was isolated by micro-dissection as previously described (Gulbransen et al., 2012), fixed overnight at 4°C in Zamboni's fixative (American MasterTech), and stained for whole-mount microscopy as previously described (Nasser et al., 2007). Briefly, following antigen retrieval and blocking, samples were incubated with successive primary and secondary antibody overnight at 4°C. Tissues were mounted in ProLong Gold Antifade mounting medium with DAPI (Life Technologies) and imaged using a Leica TCS SP8 confocal microscope. Images were collected and uniformly processed using the Leica Application Suite software. Further information and antibodies used for staining are detailed in Supplemental Experimental Procedures.

Electron Microscopy

Following euthanasia, mice were perfused with a solution of Zamboni's fixative (American MasterTech) and 0.5% glutaraldehyde. DRG and large intestine musculara were dissected and post-fixed overnight at 4°C. Following dehydration, ultrathin sections were cut on a Leica ultramicrotome, collected on Formvar-coated single-slot grids, and analyzed with a Tecnai 12 Biotwin election microscope (FEI). Images were uniformly processed to enhance the contrast using Photoshop CC (Adobe).

Histology and Immunohistochemistry

Following euthanasia, mice were perfused with a 10% solution of neutral buffered formalin. Tissues were post-fixed overnight at room temperature and then stored in 70% ethanol. Slides were prepared from paraffin embedded blocks and H&E stained or stained with anti-HSV-1/2 (Biocare Medical) by Amos Brooks of the Yale Pathology Tissue Services lab.

Peripheral Ablation of Sensory Neurons

Resiniferatoxin (RTX) was used to denervate 5- to 6-week-old female mice as previously described (Riol-Blanco et al., 2014). Briefly, mice were given escalating (30 μg/kg, 70 μg/kg, and 100 μg/kg) injections of RTX (subcutaneously) over the course of 3 days. Control mice were treated with vehicle alone (DMSO in PBS). Mice were then allowed to rest for 2 weeks before denervation was confirmed by the tail-flick assay (Le Bars et al., 2001). Mice were subsequently treated with Depo-Provera and infected with HSV-1 as described above.

Neutrophil Depletion

To deplete neutrophils, mice were treated every other day with 500 μg intraperitoneal anti-Ly6G (1A8, BioXCell) starting 5 d.p.i. and ending on 11 d.p.i. Neutrophil depletion was confirmed in the peripheral blood 24 hr after the first injection.

Detection of HSV Genome by qPCR

Dissected DRG were snap-frozen on dry ice and stored at −80°C until further processing. Tissues were thawed, and DNA was isolated using the DNeasy Blood and Tissue Kit (QIAGEN) according to the manufacturer's instructions. Relative abundance of the HSV-1 genome to the host *Tert* gene was determined by qPCR using primers listed in Supplemental Experimental Procedures.

RNA-Seq and Analysis

Total RNA from the large intestine musculara was isolated using TRIzol (Ambion) and further purified using the RNeasy RNA isolation kit (QIAGEN), both according to the manufacturer's instructions. Total RNA from the lumbosacral DRG was isolated using the RNeasy RNA isolation kit (QIAGEN). Samples were further processed and sequenced at the Yale Center for Genome Analysis. High-quality samples with a RIN score of at least 7.0 were sequenced with a 150-bp paired end read using an Illumina 2500 HiSeq sequencer. Raw sequence reads were trimmed of sequencing adaptors and low-quality regions by btrim (Kong, 2011). The trimmed reads were mapped to the mouse genome (GRCm38) by tophat2 (Kim et al., 2013), and the counts of reads for each gene were based on Ensembl annotation (release 70). After the counts were collected, the differential expression analysis was done by DEseq2

(Love et al., 2014), which calculated the adjusted p values. Differentially expressed genes with at least a 2-fold difference in expression and an adjusted p value < 0.05 were analyzed using IPA (QIAGEN). Volcano plots were constructed using ggplot2 in R with additional editing and annotating using Adobe Illustrator. For HSV-1 genes, the trimmed reads were mapped to human herpesvirus 1 genome (NC_001806.1) by bowtie2 (Langmead and Salzberg, 2012). The differential expression analysis was done by DEseq2 (Love et al., 2014) using normalization factors from host RNA-seq data for each sample. The Circos plot was generated as previously described (Krzywinski et al., 2009) and further edited and annotated using Adobe Illustrator.

Flow Cytometry

Single-cell suspensions were prepared from isolated large intestine musculara or DRG by digesting samples in a 2 mg/mL Collagenase D and 15 μg/mL DNase I solution for 15 min (DRG) or 30 min (musculara) and extruded through a 70-μm filter. Dead cells were labeled using the LIVE/DEAD Fixable Aqua Dead Cell kit (Invitrogen). Cell number was determined by CountBright absolute counting beads (Invitrogen). All samples were acquired on an LSRII equipped with a 532-nm green laser (BD Biosciences), and all data were analyzed using FlowJo software (Tree Star). Antibodies used for staining are listed in Supplemental Experimental Procedures.

ACCESSION NUMBERS

The accession number for the RNA-seq data reported in this paper is GEO: GSE74215.

SUPPLEMENTAL INFORMATION

Supplemental Information includes Supplemental Experimental Procedures and six figures and can be found with this article online at http://dx.doi.org/10.1016/j.chom.2016.05.008.

AUTHOR CONTRIBUTIONS

Conceptualization, W.K.-H., B.Y., T.L.H., and A.I.; Software and Formal Analysis. Y.K. and W.G.; Investigation, W.K.-H., B.Y., P.K., and W.G.; Resources, K.S.-B., A.R., and T.L.H.; Writing – Original Draft, W.K.-H. and A.I.; Writing – Review & Editing, W.K.-H., B.Y., Y.K., T.L.H., and A.I.; Supervision, T.L.H. and A.I.; Funding Acquisition, A.I.

ACKNOWLEDGMENTS

This work was supported by the Howard Hughes Medical Institute, National Institutes of Health (NIH) grants R01 AI081884, R01 AI054359, and R01 AI062428 (A.I.), and NIH grant T32 AI055403 (W.K.-H.). We thank Ruslan Medzhitov, Smita Gopinath, and Haina Shin for many helpful discussions.

Received: October 16, 2015
Revised: March 11, 2016
Accepted: April 23, 2016
Published: June 8, 2016

REFERENCES

Arbusow, V., Derfuss, T., Held, K., Himmelein, S., Strupp, M., Gurkov, R., Brandt, T., and Theil, D. (2010). Latency of herpes simplex virus type-1 in human geniculate and vestibular ganglia is associated with infiltration of CD8+ T cells. J. Med. Virol. *82*, 1917–1920.

Bachor, E., Bonkowsky, V., and Hacki, T. (1996). Herpes simplex virus type I reactivation as a cause of a unilateral temporary paralysis of the vagus nerve. Eur. Arch. Otorhinolaryngol. *253*, 297–300.

Boeckxstaens, G.E., and de Jonge, W.J. (2009). Neuroimmune mechanisms in postoperative ileus. Gut *58*, 1300–1311.

Brookes, S.J., Spencer, N.J., Costa, M., and Zagorodnyuk, V.P. (2013). Extrinsic primary afferent signalling in the gut. Nat. Rev. Gastroenterol. Hepatol. *10*, 286–296.

Canalejo Castrillero, E., García Durán, F., Cabello, N., and García Martínez, J. (2010). Herpes esophagitis in healthy adults and adolescents: report of 3 cases and review of the literature. Medicine (Baltimore) *89*, 204–210.

Caplan, L.R., Kleeman, F.J., and Berg, S. (1977). Urinary retention probably secondary to herpes genitalis. N. Engl. J. Med. *297*, 920–921.

Chaban, V., Christensen, A., Wakamatsu, M., McDonald, M., Rapkin, A., McDonald, J., and Micevych, P. (2007). The same dorsal root ganglion neurons innervate uterus and colon in the rat. Neuroreport *18*, 209–212.

Christianson, J.A., Liang, R., Ustinova, E.E., Davis, B.M., Fraser, M.O., and Pezzone, M.A. (2007). Convergence of bladder and colon sensory innervation occurs at the primary afferent level. Pain *128*, 235–243.

Chu-Wang, I.W., and Oppenheim, R.W. (1978). Cell death of motoneurons in the chick embryo spinal cord. I. A light and electron microscopic study of naturally occurring and induced cell loss during development. J. Comp. Neurol. *177*, 33–57.

Daley, J.M., Thomay, A.A., Connolly, M.D., Reichner, J.S., and Albina, J.E. (2008). Use of Ly6G-specific monoclonal antibody to deplete neutrophils in mice. J. Leukoc. Biol. *83*, 64–70.

De Giorgio, R., Ricciardiello, L., Naponelli, V., Selgrad, M., Piazzi, G., Felicani, C., Serra, M., Fronzoni, L., Antonucci, A., Cogliandro, R.F., et al. (2010). Chronic intestinal pseudo-obstruction related to viral infections. Transplant. Proc. *42*, 9–14.

Debinski, H.S., Kamm, M.A., Talbot, I.C., Khan, G., Kangro, H.O., and Jeffries, D.J. (1997). DNA viruses in the pathogenesis of sporadic chronic idiopathic intestinal pseudo-obstruction. Gut *41*, 100–106.

Fleck, M., Podlech, J., Weise, K., Müntefering, H., and Falke, D. (1993). Pathogenesis of HSV-1/2 induced vaginitis/vulvitis of the mouse: dependence of lesions on genetic properties of the virus and analysis of pathohistology. Arch. Virol. *129*, 35–51.

Gesser, R.M., and Koo, S.C. (1996). Oral inoculation with herpes simplex virus type 1 infects enteric neuron and mucosal nerve fibers within the gastrointestinal tract in mice. J. Virol. *70*, 4097–4102.

Gesser, R.M., Valyi-Nagy, T., Altschuler, S.M., and Fraser, N.W. (1994). Oral-oesophageal inoculation of mice with herpes simplex virus type 1 causes latent infection of the vagal sensory ganglia (nodose ganglia). J. Gen. Virol. *75*, 2379–2386.

Goodell, S.E., Quinn, T.C., Mkrtichian, E., Schuffler, M.D., Holmes, K.K., and Corey, L. (1983). Herpes simplex virus proctitis in homosexual men. Clinical, sigmoidoscopic, and histopathological features. N. Engl. J. Med. *308*, 868–871.

Gulbransen, B.D., Bashashati, M., Hirota, S.A., Gui, X., Roberts, J.A., MacDonald, J.A., Muruve, D.A., McKay, D.M., Beck, P.L., Mawe, G.M., et al. (2012). Activation of neuronal P2X7 receptor-pannexin-1 mediates death of enteric neurons during colitis. Nat. Med. *18*, 600–604.

Johnson, A.J., Chu, C.F., and Milligan, G.N. (2008). Effector CD4+ T-cell involvement in clearance of infectious herpes simplex virus type 1 from sensory ganglia and spinal cords. J. Virol. *82*, 9678–9688.

Kastrukoff, L.F., Lau, A.S., and Puterman, M.L. (1986). Genetics of natural resistance to herpes simplex virus type 1 latent infection of the peripheral nervous system in mice. J. Gen. Virol. *67*, 613–621.

Kim, D., Pertea, G., Trapnell, C., Pimentel, H., Kelley, R., and Salzberg, S.L. (2013). TopHat2: accurate alignment of transcriptomes in the presence of insertions, deletions and gene fusions. Genome Biol. *14*, R36.

Knickelbein, J.E., Khanna, K.M., Yee, M.B., Baty, C.J., Kinchington, P.R., and Hendricks, R.L. (2008). Noncytotoxic lytic granule-mediated CD8+ T cell inhibition of HSV-1 reactivation from neuronal latency. Science *322*, 268–271.

Kong, Y. (2011). Btrim: a fast, lightweight adapter and quality trimming program for next-generation sequencing technologies. Genomics *98*, 152–153.

Kramer, T., and Enquist, L.W. (2012). Alphaherpesvirus infection disrupts mitochondrial transport in neurons. Cell Host Microbe *11*, 504–514.

Krzywinski, M., Schein, J., Birol, I., Connors, J., Gascoyne, R., Horsman, D., Jones, S.J., and Marra, M.A. (2009). Circos: an information aesthetic for comparative genomics. Genome Res. *19*, 1639–1645.

Langmead, B., and Salzberg, S.L. (2012). Fast gapped-read alignment with Bowtie 2. Nat. Methods *9*, 357–359.

Le Bars, D., Gozariu, M., and Cadden, S.W. (2001). Animal models of nociception. Pharmacol. Rev. *53*, 597–652.

Leib, D.A., Alexander, D.E., Cox, D., Yin, J., and Ferguson, T.A. (2009). Interaction of ICP34.5 with Beclin 1 modulates herpes simplex virus type 1 pathogenesis through control of CD4+ T-cell responses. J. Virol. *83*, 12164–12171.

Looker, K.J., Magaret, A.S., May, M.T., Turner, K.M., Vickerman, P., Gottlieb, S.L., and Newman, L.M. (2015a). Global and Regional Estimates of Prevalent and Incident Herpes Simplex Virus Type 1 Infections in 2012. PLoS ONE *10*, e0140765.

Looker, K.J., Magaret, A.S., Turner, K.M., Vickerman, P., Gottlieb, S.L., and Newman, L.M. (2015b). Global estimates of prevalent and incident herpes simplex virus type 2 infections in 2012. PLoS ONE *10*, e114989.

Lopez, C. (1975). Genetics of natural resistance to herpesvirus infections in mice. Nature *258*, 152–153.

Love, M.I., Huber, W., and Anders, S. (2014). Moderated estimation of fold change and dispersion for RNA-seq data with DESeq2. Genome Biol. *15*, 550.

Malkin, J.E. (2004). Epidemiology of genital herpes simplex virus infection in developed countries. Herpes *11*, 2A–23A.

Nasser, Y., Keenan, C.M., Ma, A.C., McCafferty, D.M., and Sharkey, K.A. (2007). Expression of a functional metabotropic glutamate receptor 5 on enteric glia is altered in states of inflammation. Glia *55*, 859–872.

Parr, M.B., and Parr, E.L. (2003). Intravaginal administration of herpes simplex virus type 2 to mice leads to infection of several neural and extraneural sites. J. Neurovirol. *9*, 594–602.

Parr, M.B., Kepple, L., McDermott, M.R., Drew, M.D., Bozzola, J.J., and Parr, E.L. (1994). A mouse model for studies of mucosal immunity to vaginal infection by herpes simplex virus type 2. Lab. Invest. *70*, 369–380.

Price, R.W. (1977). Viral infections of the autonomic nervous system and its target organs: pathogenetic mechanisms. Med. Hypotheses *3*, 33–36.

Reinert, L.S., Harder, L., Holm, C.K., Iversen, M.B., Horan, K.A., Dagnæs-Hansen, F., Ulhøi, B.P., Holm, T.H., Mogensen, T.H., Owens, T., et al. (2012). TLR3 deficiency renders astrocytes permissive to herpes simplex virus infection and facilitates establishment of CNS infection in mice. J. Clin. Invest. *122*, 1368–1376.

Richter, E.R., Dias, J.K., Gilbert, J.E., 2nd, and Atherton, S.S. (2009). Distribution of herpes simplex virus type 1 and varicella zoster virus in ganglia of the human head and neck. J. Infect. Dis. *200*, 1901–1906.

Riol-Blanco, L., Ordovas-Montanes, J., Perro, M., Naval, E., Thiriot, A., Alvarez, D., Paust, S., Wood, J.N., and von Andrian, U.H. (2014). Nociceptive sensory neurons drive interleukin-23-mediated psoriasiform skin inflammation. Nature *510*, 157–161.

Shin, H., and Iwasaki, A. (2012). A vaccine strategy that protects against genital herpes by establishing local memory T cells. Nature *491*, 463–467.

Shin, H., and Iwasaki, A. (2013). Tissue-resident memory T cells. Immunol. Rev. *255*, 165–181.

Simmons, A., and Tscharke, D.C. (1992). Anti-CD8 impairs clearance of herpes simplex virus from the nervous system: implications for the fate of virally infected neurons. J. Exp. Med. *175*, 1337–1344.

Stock, A.T., Smith, J.M., and Carbone, F.R. (2014). Type I IFN suppresses Cxcr2 driven neutrophil recruitment into the sensory ganglia during viral infection. J. Exp. Med. *211*, 751–759.

Tsukamoto, T., Antonic, V., El Hajj, I.I., Stojadinovic, A., Binion, D.G., Izadjoo, M.J., Yokota, H., Pape, H.C., and Bauer, A.J. (2011). Novel model of peripheral tissue trauma-induced inflammation and gastrointestinal dysmotility. Neurogastroenterol. Motil. *23*, 379–386.

Virgin, H.W., Wherry, E.J., and Ahmed, R. (2009). Redefining chronic viral infection. Cell *138*, 30–50.

Wald, A., Zeh, J., Selke, S., Ashley, R.L., and Corey, L. (1995). Virologic characteristics of subclinical and symptomatic genital herpes infections. N. Engl. J. Med. *333*, 770–775.

Warren, K.G., Brown, S.M., Wroblewska, Z., Gilden, D., Koprowski, H., and Subak-Sharpe, J. (1978). Isolation of latent herpes simplex virus from the superior cervical and vagus ganglions of human beings. N. Engl. J. Med. *298*, 1068–1069.

Whitely, R.J., Kimberlin, D.W., and Bernard, R. (1998). Herpes simplex viruses. Clin. Infect. Dis. *26*, 541–555.

Yordy, B., Iijima, N., Huttner, A., Leib, D., and Iwasaki, A. (2012). A neuron-specific role for autophagy in antiviral defense against herpes simplex virus. Cell Host Microbe *12*, 334–345.